Surface State Charge Dynamics of a High-Mobility Three-Dimensional Topological Insulator

Jason N. Hancock,[1] J. L. M. van Mechelen,[1] Alexey B. Kuzmenko,[1] Dirk van der Marel,[1] Christophe Brüne,[2] Elena G. Novik,[2] Georgy V. Astakhov,[2] Hartmut Buhmann,[2] and Laurens W. Molenkamp[2]

[1]*Département de Physique de la Matière Condensée, Université de Genève, quai Ernest-Ansermet 24, CH 1211 Genève 4, Switzerland*

[2]*Physikalisches Institut der Universität Würzburg - 97074 Würzburg, Germany*

(Received 12 May 2011; revised manuscript received 14 July 2011; published 21 September 2011)

We present a magneto-optical study of the three-dimensional topological insulator, strained HgTe, using a technique which capitalizes on advantages of time-domain spectroscopy to amplify the signal from the surface states. This measurement delivers valuable and precise information regarding the surface-state dispersion within <1 meV of the Fermi level. The technique is highly suitable for the pursuit of the topological magnetoelectric effect and axion electrodynamics.

DOI: 10.1103/PhysRevLett.107.136803 PACS numbers: 73.25.+i, 03.65.Vf, 73.20.Mf, 78.20.Ls

Spin 1/2 particles exhibit the counterintuitive property that their wave function acquires a π phase upon 360° rotation. If spin and orbital degrees of freedom are mixed in a particular way, the momenta of electrons in a crystalline lattice feel important effects of this π ''Berry's phase,''which can lead to a new phase of matter whose description requires a fundamental redress of the theory of semiconductors [1–3], and probably many other materials classes [4–6]. These topological insulators exhibit an odd number of metallic surface bands with helical spin texture [7–9] surrounding the nominally insulating bulk and display characteristic suppression of backscattering from step edges and nonmagnetic impurities [10,11]. We present magneto-optical measurements deep in the terahertz frequency regime exploring the charge dynamics of surface states in high-mobility strained films of HgTe [12–15]. Using a time-domain technique, we detect a strong magneto-optical signal which is dominated by surface bands. This information reveals precise details of the low-energy excitations and momentum-energy dispersion of the helical metallic surface state.

The observation of the quantum spin Hall effect (QSHE) in CdTe-HgTe-CdTe quantum wells [16,17] represents a significant advance in the ability to robustly segregate electronic currents of opposite spin, an effect which paves the way to new applications for spintronics and fault-tolerant quantum computation. In bulk, HgTe possesses the band inversion property due to spin-orbit interaction, a prerequisite condition for the QSHE, but also needed to realize a three-dimensional topological insulator phase. Unfortunately, the Fermi level appears directly at the intersection of two bands, rendering the bulk semimetallic and leaving the surface states and the expected topological aspects of this material obscured by the low-energy bulk excitations. However, when HgTe is compressively strained against a CdTe substrate, the bulk band intersection becomes fully gapped in response to the lowered symmetry, permitting isolated access to helical surface bands [12–15]. Recently, strong evidence for the existence of the π Berry's phase, surface bands, and the associated zero Landau level was observed as a quantum Hall effect of surface states, whose existence was subsequently verified using angle-resolved photoemission [15].

In order to directly probe the surface states of strained HgTe, we have developed a method of acquiring time-domain terahertz magneto-optical data using a home-built superconducting magnet in a flow cryostat, illustrated in Fig. 1(a). Complementary to frequency-domain measurements performed on the same sample at higher temperature (>50 K) [18], which were interpreted in terms of a thermally activated carriers in the bulk, our measurements were performed at low temperature, where the terahertz response is due to a combination of intrinsically doped bulk carriers and topological surface bands [15]. At 4.35 K, the magnetic field and incident polarizer angle θ_P were set, and one direct pulse plus one echo, due to internal reflection inside the substrate, were collected for analyzer angles θ_A subtending 400° in 10° steps. The pulse and echo were then partitioned into $E_1(t, \theta_A, B)$ and $E_2(t, \theta_A, B)$ as shown in Fig. 1(b), and separately Fourier transformed to obtain the electric field amplitudes $E_1(\omega, \theta_A, B)$ and $E_2(\omega, \theta_A, B)$.

When the pulse passes through or reflects from the film, the electric field direction can rotate due to off-diagonal elements of the dielectric tensor or possibly the predicted topological magnetoelectric effect [19]. Accounting for the horizontally polarizing detector and emitter antenna of the spectrometer, the electric field amplitude in pulse i at the detector is

$$E_i = E_s \cos\theta_P \cos\theta_A \cos(\theta_A - \theta_P + \theta_{F,i}) \qquad (1)$$

where E_s is the electric field generated by the source and $\theta_{F,i}$ is the complex, sample-induced Faraday rotation of the ith pulse. Figures 1(d) and 1(e) show exemplary fits of Eq. (1) to the measured intensity of the second pulse $|E_2(\omega, \theta_A, \pm 1.4T)|^2$ and different frequencies. The change in shape of the intensity distribution around 35 cm^{-1} is

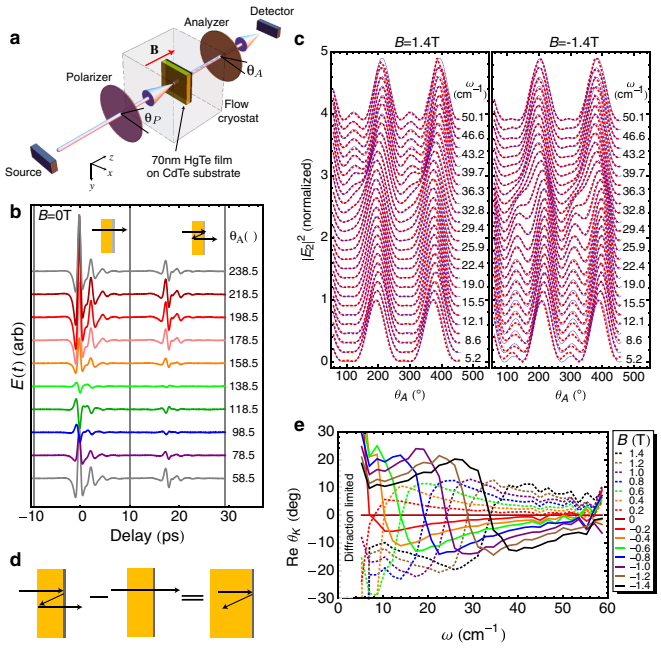

FIG. 1 (color online). Time-domain measurement of the normal-incidence Kerr angle. (a) Illustration of the magneto-optical THz apparatus. θ_P was set to 51.2° throughout. (b) Subset of the angle-dependent measurements of the 1st and 2nd pulses. Vertical lines show the cuts used to separate the pulses into E_1 and E_2. (c) Measured $|E_2|^2$ (red dashes) and the fit from Eq. (1) (blue lines) used to determine the Faraday angle $\theta_{F,2}(\omega)$ for $+1.4T$ and $-1.4T$. (d) Pictorial rationale for the expression $\theta_{F,2} - \theta_{F,1} = \theta_K$. (e) The measured θ_K for several magnetic field values.

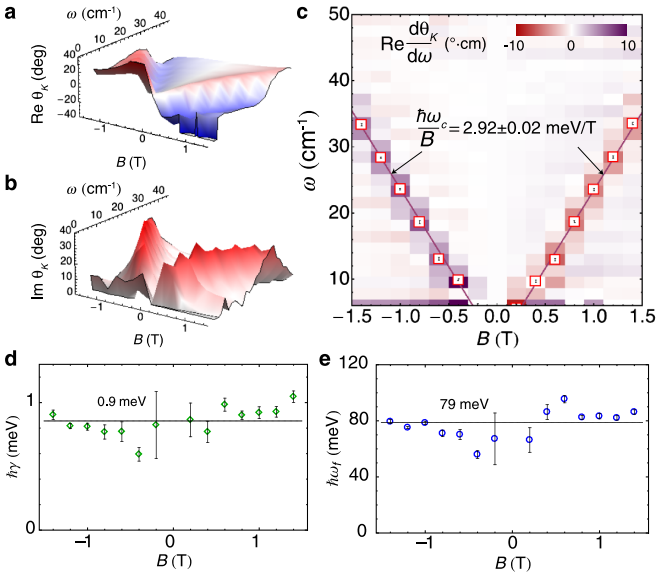

FIG. 2 (color online). Properties of the surface-state cyclotron resonance. Real (a) and imaginary (b) Kerr angle $\theta_K(\omega, B)$ determined from terahertz ellipsometry. (c) The experimentally determined ω_c (red squares) and a linear fit (purple lines) showing the B-linear CR behavior. ω_c corresponds to the inflections in $\mathrm{Re}\theta_K(\omega)$, as demonstrated by the experimental frequency derivative $\mathrm{Re}d\theta_K/d\omega$, shown as a false color plot in the background. (d),(e) Fit parameters γ and ω_f. The error bars arise from scatter in the determined CR parameters.

caused by a change in the complex Faraday angle $\theta_{F,2}$ at this frequency, which we attribute to an absorptive transition among surface-state Landau levels. The fitting procedure was applied to both pulses to uniquely determine $\theta_{F,1}$ and $\theta_{F,2}$ at each frequency and field value measured.

The simultaneous acquisition of multiple pulses with separate histories of contact with the film provides an advantage in accurately determining the polarization rotation due to the film. Any polarizing effects of the polyethylene cryostat windows as well as inaccuracy in repositioning the polarizer following an angle sweep is exactly the same for the two pulses, so taking the difference in the two Faraday angles $\theta_K = \theta_{F,2} - \theta_{F,1}$ cancels these extraneous effects [20]. A separate measurement of a reference CdTe substrate showed negligible rotation in magnetic field, and this normal-incidence Kerr angle θ_K, shown in Figs. 1(e), 2(a), and 2(b) is precisely the rotation of polarization induced when the pulse reflects at normal incidence from the substrate side of the film [Fig. 1(d)], and the accuracy to which it can be determined is greater than for the Faraday angles separately.

The field-induced changes in θ_K are typical of cyclotron resonance (CR) behavior, for which the dynamical conductivity appropriate for photon angular momentum either parallel (+) or antiparallel (−) the momentum of the incident photon is:

$$\sigma_{\pm}(\omega) = i\frac{e^2}{h}\sum_j \frac{\omega_f^j}{\omega \pm \omega_c^j + i\gamma} \tag{2}$$

where ω_c^j is the cyclotron frequency, ω_f^j the Drude weight, and γ^j is the inverse lifetime of the jth band. The elementary response functions in Eq. (2) are then plugged into the expression

$$\tan\theta_K = -\frac{iZ_0 n_s(\sigma_+ - \sigma_-)}{n_s^2 - (1 + Z_0\sigma_+)(1 + Z_0\sigma_-)}$$

to fit the measured Kerr angle. Here, n_s is the measured substrate index of refraction and Z_0 is the impedance of free space (see Supplemental Material [21]). While we explore the possibility of a multicomponent CR below, the resonance at each field is fit and satisfactorily described by a single effective ω_c, γ, and ω_f. This procedure results in the parameters summarized in Figs. 2(c)–2(e). The sign of the rotation indicates that the carriers involved in the CR are electronlike, and fits to the field dependence give $\hbar\gamma = 0.9$ meV, a field-linear cyclotron frequency with $\hbar\omega_c/B = 2.92 \pm 0.02$ meV/T, and total Drude weight $\hbar\omega_f = 79.0 \pm 1.7$ meV. Using the relation $\mu B = \omega_c/\gamma$, and the nearly field-independent γ [Fig. 2(d)], these fits imply a very high carrier mobility $\mu = 34,220$ cm^2/V s,

consistent with previous transport [15] and optical [18] measurements.

In the limit of small carrier concentration, which as we will see below is the relevant limit in the context of this discussion, the 2D Fermi surfaces are isotropic, and ω_f^j and ω_c^j at low fields are uniquely determined by the Fermi momentum, k_F^j, and the group velocity at the Fermi energy, v_F^j (see [21])

$$\omega_f^j = \frac{1}{2} v_F^j k_F^j \qquad \omega_c^j = \frac{eB}{\hbar} \frac{v_F^j}{k_F^j}.$$

Knowledge of ω_f^j and ω_c^j therefore permits determination of the parameters v_F^j and k_F^j, which in turn provides valuable and precise information on the band structure at and around the Fermi energy.

In our 70 nm films, the conduction band is quantized and well separated in energy due to confinement in the z direction, and at low temperature any possible bulk contributions come from a small number of two-dimensional electron pockets. Unlike bulk, the surface contributions to the Drude weight are present for all values of the chemical potential, due to their gapless nature. Because the surface bands are at higher filling ($k_F^s > k_F^b$) and are more steeply dispersing ($v_F^s > v_F^b$) than the conduction bands, these states not only always contribute to the CR, but also always contribute more strongly to the magneto-optical signal than a set of bulk states with the same Fermi surface area.

Before we address the implications of possible contributions from the bulk, we start with the simplest assumption, namely, that the only contributions to the observed Kerr rotation originate from the two surfaces of the film with approximately the same charge carrier concentration. This is motivated by the magnetotransport showing a quantized Hall effect that results from the 2D Dirac-like topological surface states with densities 4.8×10^{11} cm^{-2} and 3.7×10^{11} cm^{-2} for the CdTe and vacuum interfaces (respectively) and negligible contribution from the bulk [15]. Since with this assumption $\hbar\omega_f^j = 39.5 \pm 0.9$ meV for the two surfaces, combination with ω_c/B gives $v_F^s = 5.88 \times 10^5$ m/s and $k_F^s = 0.201$ nm^{-1} [see Fig. 3(a)]. The corresponding carrier concentration per surface is $n_{2D} = k_F^2/(4\pi) = 3.2 \times 10^{11}$ cm^{-2} in good agreement with the high field transport data [15] and strongly evidencing a surface-dominated origin of the CR signal. The remaining difference is within the observed variations from one cooldown to another of the same sample, which we attribute to molecular adsorption at the surface of the film at cryogenic temperatures. Comparing these k_F values with the quantum well band structure in [15], the level of the chemical potential should be positioned above the conduction band bottom with 25% of the Drude weight arising from the bulk states of the film, with the remainder due to the surface bands. Attributing only 75% of the observed Drude weight to the surface states would result in: $v_F^s = 5.09 \times 10^5$ m/s and $k_F^s = 0.174$ nm^{-1}, as indicated by the green (light gray) dashed line in Fig. 3(a). Angle-resolved photoelectron spectroscopy shows a linear dispersion down to 1 eV below the Fermi energy with a velocity 4.3×10^5 m/s [15]. The somewhat higher value obtained from the optical data is expected, since this probes the velocity at the Fermi energy which is closer to

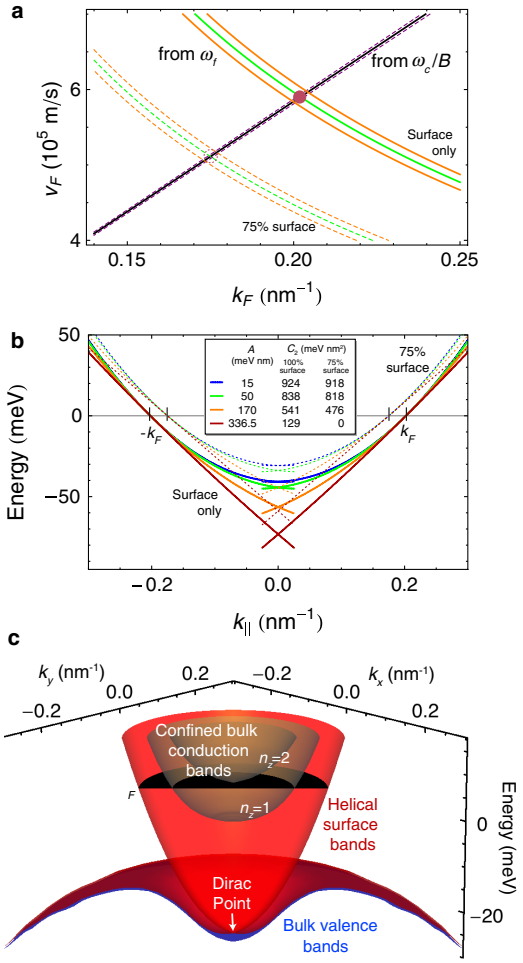

FIG. 3 (color online). Dispersion of the surface-state band. (a) Constraints on Fermi parameters k_F and v_F consistent with the magneto-optical data. Black line shows the constraint from the observed ω_c/B, and purple dashes indicate the error bars on this quantity. Green (light gray) solid curve is a constraint from the observed ω_f assuming the CR is due solely to two identical surface states at the surface and interface, with solid orange (medium gray) curves indicating the error bars. Dashed orange (medium gray) and green (light gray) curves show the effect of breaking this assumption and allowing 25% of the Drude weight to be attributed to the confined conduction band states. (b) Possible realizations of a minimal surface-state model in [22] which are consistent with our observations for different choices of A and C_2. The Fermi level μ_F, shown in black, intersects the surface and confined bulk conduction subbands. (c) Dispersion of the surface-state quasiparticles determined in this work with a 75% surface-state signal, $A = 25$ meV nm, and $C_2 = 890$ meV nm^2.

the light conduction bands hybridizing with the 2D surface states.

A more detailed perspective of the surface-dominated cyclotron resonance can be attained through comparison of these results to a surface-state model dispersion relation $\epsilon_k = E_{\mathrm{DP}} + Ak + C_2k^2$ [22]. This form accommodates the topologically protected Dirac point (DP) through the A term, but allows for significant deviations from the ideal conical dispersion through the C_2 term. By varying these parameters, one can interpolate continuously between a pure Dirac cone ($C_2 \rightarrow 0$) and a parabola ($A \rightarrow 0$) emanating from the Dirac point at zone center and energy E_{DP} lying inside the bulk gap. All of the curves of this type with the same values of k_F and v_F fit equally well to our data, as shown in Fig. 3(b). However, in order to place the DP inside the bulk gap, estimated to be $\sim$26 meV at zone center [15], the A parameter must be very small, $A < 50$ meV $\cdot$ nm, to be consistent with our data. The resultant parameter C_2 is therefore quite large in comparison to other topological materials [7–9,22], indicating a relatively rapid departure from the ideal conical dispersion near the DP in strained HgTe. The large second-order term leads one to suspect that higher order isotropic terms (k^3, $k^4, \ldots$) may be necessary for detailed analysis of certain experiments.

While we do not measure the Fermi energy directly, the simplified dispersion analysis above puts the chemical potential within 40 meV of the Dirac point. This difference can be overcome through gating in an appropriate experimental design, and the chemical potential can be tuned near the Zeeman split zero Landau level. This would fulfill the conditions required to observe the predicted topological magnetoelectric coupling effect [19,23] as a quantized Kerr rotation. This long-sought effect bears close mathematical analogy to high-energy particle theory, permitting one to use terahertz spectroscopy to study the properties of an ''axion'' domain wall [24], and the methods developed here are highly suited for this pursuit.

We have studied the low-energy electrodynamics of topological surface states of strained HgTe using a novel time-domain magneto-optical spectroscopic technique providing Kerr angle spectra to very low energies (< 1 meV). The method allowed us to obtain the parameters describing the topological surface states near the Fermi energy, until now not resolved by other experimental techniques, namely, free carrier spectral weight, quasiparticle scattering rate, cyclotron frequency, Fermi velocity and Fermi momentum. Taken together with the requirement that the Dirac point must lie inside the bulk gap, our results imply that the surface bands of strained HgTe are markedly nonconical.

We acknowledge valuable discussions with Shoucheng Zhang and Alberto Morpurgo. This work is supported by the SNSF through Grant No. 200020-135085 and the National Center of Competence in Research (NCCR) MaNEP.

[1] C. L. Kane and E. J. Mele, Phys. Rev. Lett. **95**, 226801 (2005).
[2] H. Zhang, C.-X. Liu, X.-L. Qi, X. Dai, Z. Fang, and S.-C. Zhang, Nature Phys. **5**, 438 (2009).
[3] M. Z. Hasan and C. L. Kane, Rev. Mod. Phys. **82**, 3045 (2010).
[4] S. Raghu, X.-L. Qi, C. Honerkamp, and S.-C. Zhang, Phys. Rev. Lett. **100**, 156401 (2008).
[5] C. W. Groth, M. Wimmer, A. R. Akhmerov, J. Tworzydło, and C. W. J. Beenakker, Phys. Rev. Lett. **103**, 196805 (2009).
[6] M. Dzero, K. Sun, V. Galitski, and P. Coleman, Phys. Rev. Lett. **104**, 106408 (2010).
[7] D. Hsieh, D. Qian, L. Wray, Y. Xia, Y. S. Hor, R. J. Cava, and M. Z. Hasan, Nature (London) **452**, 970 (2008).
[8] D. Hsieh, Y. Xia, D. Qian, L. Wray, J. H. Dil, F. Meier, J. Osterwalder, L. Patthey, J. G. Checkelsky, and N. P. Ong *et al.*, Nature (London) **460**, 1101 (2009).
[9] Y. L. Chen, J. G. Analytis, J.-H. Chu, Z. K. Liu, S.-K. Mo, X. L. Qi, H. J. Zhang, D. H. Lu, X. Dai, and Z. Fang *et al.*, Science **325**, 178 (2009).
[10] Z. Alpichshev, J. G. Analytis, J.-H. Chu, I. R. Fisher, Y. L. Chen, Z. X. Shen, A. Fang, and A. Kapitulnik, Phys. Rev. Lett. **104**, 016401 (2010).
[11] P. Roushan, J. Seo, C. V. Parker, Y. S. Hor, D. Hsieh, D. Qian, A. Richardella, M. Z. Hasan, R. J. Cava, and A. Yazdani, Nature (London) **460**, 1106 (2009).
[12] L. Fu and C. L. Kane, Phys. Rev. B **76**, 045302 (2007).
[13] X. Dai, T. L. Hughes, X.-L. Qi, Z. Fang, and S.-C. Zhang, Phys. Rev. B **77**, 125319 (2008).
[14] J.-W. Luo and A. Zunger, Phys. Rev. Lett. **105**, 176805 (2010).
[15] C. Brüne, C. X. Liu, E. G. Novik, E. M. Hankiewicz, H. Buhmann, Y. L. Chen, X. L. Qi, Z. X. Shen, S. C. Zhang, and L. W. Molenkamp, Phys. Rev. Lett. **106**, 126803 (2011).
[16] B. A. Bernevig, T. L. Hughes, and S.-C. Zhang, Science **314**, 1757 (2006).
[17] M. König, S. Wiedmann, C. Brüne, A. Roth, H. Buhmann, L. W. Molenkamp, X.-L. Qi, and S.-C. Zhang, Science **318**, 766 (2007).
[18] A. M. Shuvaev, G. V. Astakhov, A. Pimenov, C. Brüne, H. Buhmann, and L. W. Molenkamp, Phys. Rev. Lett. **106**, 107404 (2011).
[19] X.-L. Qi, T. L. Hughes, and S.-C. Zhang, Phys. Rev. B **78**, 195424 (2008).
[20] This interpretation of the difference angle is possible because the CdTe substrate showed negligible rotation under similar conditions.
[21] See Supplemental Material at http://link.aps.org/supplemental/10.1103/PhysRevLett.107.136803 for the measured refractive index $n_s(\omega)$ of CdTe, quality of fits to θ_K, and derivation of relevant equations presented in the text.
[22] C.-X. Liu, X.-L. Qi, H. J. Zhang, X. Dai, Z. Fang, and S.-C. Zhang, Phys. Rev. B **82**, 045122 (2010).
[23] W.-K. Tse and A. H. MacDonald, Phys. Rev. Lett. **105**, 057401 (2010).
[24] F. Wilczek, Phys. Rev. Lett. **58**, 1799 (1987).

Surface state charge dynamics of a bulk carrier-free three dimensional topological insulator (Supplemental Materials)

Jason N. Hancock[1], J. L. M. van Mechelen[1], Alexey B. Kuzmenko[1], Dirk van der Marel[1], C. Brüne[2], E. G. Novik[2], G. V. Astakhov[2], H. Buhmann[2], Laurens Molenkamp[2]

[1] *Département de Physique de la Matière Condensée, Université de Genève, quai Ernest-Ansermet 24, CH 1211 Genève 4, Switzerland and*

[2] *Physikalisches Institut der Universität Würzburg - 97074 Würzburg, Germany*

Materials and methods

High mobility, 70 nm HgTe film sample was grown on a thick CdTe substrate using molecular beam epitaxy, and characterized by X-ray, ARPES, and d. c. transport measurements. The finite area of the film, 4×5 mm, limits the lowest measurable frequency in our measurements. Time-domain terahertz traces were collected with a commercial system employing a mode-locked laser and photoconducting antennae.

Magneto-optical THz measurements

Equation (1) of the main text is an example of Malus' law, and is straightforward to derive.

For a given angular momentum state of the photon (+ or -), the transmission coefficient is

$$t_{1,\pm} = t_{vs} e^{i\phi_s} t_{sfv,\pm} \tag{1}$$

for the first pulse and

$$t_{2,\pm} = t_{vs} e^{3i\phi_s} r_{sfv,\pm} r_{sv} t_{sfv,\pm} \tag{2}$$

for the second pulse, where

$$t_{vs} = \frac{2}{n_s + 1} \tag{3}$$

$$r_{sv} = \frac{n_s - 1}{n_s + 1} \tag{4}$$

are the usual Fresnel coefficients for transmission and reflection at the substrate/vacuum interface, ϕ_s is the complex phase shift acquired through traversal across the substrate and s, f, and v stand for substrate, film, and vacuum, respectively.

The coefficients which include the thin film are

$$t_{sfv,\pm} = \frac{2n_s}{n_s + 1 + Z_0\sigma_\pm} \tag{5}$$

$$r_{sfv,\pm} = \frac{n_s - 1 - Z_0\sigma_\pm}{n_s + 1 + Z_0\sigma_\pm} \tag{6}$$

where $Z_0 = \sqrt{\mu_0/\epsilon_0} \simeq 376.63...\ \Omega$ is the impedance of free space. The Faraday angle of the ith pulse $\theta_{F,i}$ is

$$\tan\theta_{F,i} = -i\frac{t_{i,+} - t_{i,-}}{t_{i,+} + t_{i,-}} \tag{7}$$

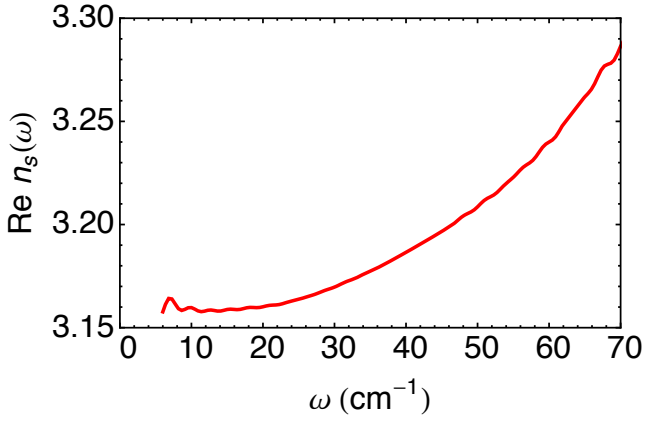

FIG. 1: Index of refraction of a CdTe substrate measured using terahertz spectroscopy and used to fit the normal incidence Kerr angle θ_K to the cyclotron resonance formulae (Eqn 2, main text).

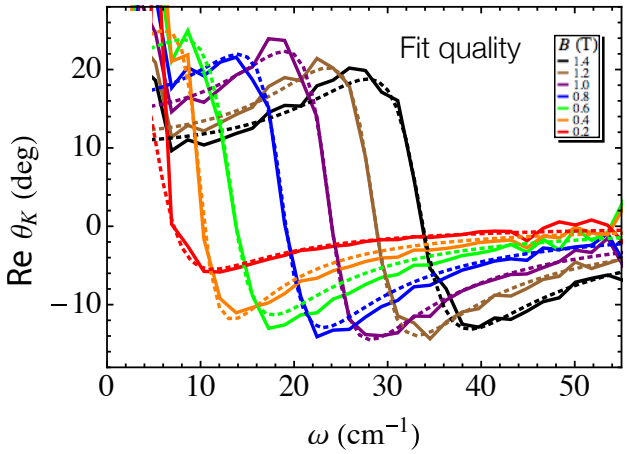

FIG. 2: Fit quality of the CR formula to the measured Reθ_K for positive fields.

Using a trigonometric identity,

$$\tan\theta_K = \tan\left(\theta_{F,2} - \theta_{F,1}\right) = -\frac{iZ_0 n_s(\sigma_+ - \sigma_-)}{n_s^2 - (1 + Z_0\sigma_+)(1 + Z_0\sigma_-)} \tag{8}$$

This relation connects the model conductivity to the measured normal-incidence Kerr angle. The frequency-dependent index of refraction of the substrate was determined from separate measurements and is shown in Figure 1. The quality of fit used to deduce ω_c, ω_f, and γ is shown for positive fields in Figure 2.

Drude weight and cyclotron frequency, general considerations

For isotropic planar dispersion, the Drude weight of a band i is

$$\omega_f^i = \frac{1}{2\pi}\oint_{FS}\frac{v_F^i(k)^2}{|\vec{v}_F^i(k)|}dk = \frac{1}{2\pi}\frac{v_F^i}{2}(2\pi k_F^i) = \frac{1}{2}v_F^i k_F^i \tag{9}$$

The frequency ω of electrons executing closed orbits of k-space area A satisfies [1]

$$\frac{1}{B} = \frac{2\pi e}{\hbar^2\omega}\frac{\partial\epsilon}{\partial A}n \tag{10}$$

where the cyclotron frequency ω_c corresponds to the first harmonic ($n = 1$).

In our case of an isotropic 2D Fermi surface,

$$A = \pi k_F^2 \tag{11}$$

We use the fact that $d\epsilon/dk = \hbar v$ is the group velocity, so that

$$\frac{\partial A}{\partial\epsilon} = 2\pi\frac{k_F}{\hbar v_F} \tag{12}$$

from which

$$\hbar\omega_c = eB\frac{v_F}{k_F}. \tag{13}$$

Surface state model

The surface state model is given in reference [2] as

$$\epsilon_s(k) = E_{DP} + Ak + C_2k^2. \tag{14}$$

The Fermi wavevector is

$$k_F^s = \frac{-A + \sqrt{A^2 + 4C_2(\mu_F - E_{DP})}}{2C_2}. \tag{15}$$

and the Fermi velocity is

$$\hbar v_F^s = A + 2C_2k_F^s. \tag{16}$$

[1] N. W. Ashcroft and N. D. Mermin, *Solid State Physics* (Brooks Cole, 1976), 1st ed., ISBN 0030839939.

[2] C.-X. Liu, X.-L. Qi, H. Zhang, X. Dai, Z. Fang, and S.-C. Zhang, Phys. Rev. B **82**, 045122 (2010).